Modulational instability of nonlinear spin waves in easy-axis antiferromagnetic chains

R. Lai and A. J. Sievers
Laboratory of Atomic and Solid State Physics and Materials Science Center, Cornell University, Ithaca, New York 14853-2501
(Received 30 July 1997; revised manuscript received 15 September 1997)

The modulational instability of extended nonlinear spin waves in antiferromagnetic chains with on-site easy-axis anisotropy has been investigated both analytically in the frame of linear-stability analysis and numerically by means of molecular-dynamics simulations. The linear-stability analysis predicts the instability region and the growth rates of modulation satellites. Our numerical simulations demonstrate that the analytical predictions correctly describe the onset of instability. For long-time scales when the instability is fully developed the linear-stability analysis fails and the modulated nonlinear spin waves can evolve into localized excitations. We explore the possibility of generating intrinsic localized spin-wave modes from extended spin waves through modulational instability and find that both discreteness *and* strong nonlinearity seem to be essential for the creation of long-lived localized excitations. The addition of weak dissipation is found to impose a finite amplitude threshold even for infinite chains. [S0163-1829(98)04806-1]

I. INTRODUCTION

Since the early evidence that intrinsic localized vibrational modes in anharmonic crystals should represent robust solutions,[1–4] the idea of intrinsic localization in various nonintegrable discrete lattices continues to be tested.[5–7] It is now established that intrinsic localized modes are ubiquitous to many homogeneous nonlinear lattices with the first rigorous proof for the existence of intrinsic localized modes in a wide class of models presented for the anticontinuous limit.[8–10] However, the question of how the atomic scale large-amplitude excitation can be created in homogeneous discrete lattices is still open. Modulational instability (MI), which refers to the exponential growth of certain modulation sidebands of nonlinear plane waves propagating in a dispersive medium as a result of the interplay between nonlinearity and dispersion effect, has been studied in a variety of fields.[11–14] In most of these cases, MI appears in continuous media where the propagation of nonlinear waves is usually governed by nonlinear Schrödinger-type partial differential equations. These studies of continuum models have shown that the initial amplitude of an unstable modulation wave grows exponentially with the time evolution of a modulated nonlinear plane wave. Although the onset of MI can be quantitatively described by linear-stability analysis, the long-time behavior is analytically untractable. Nevertheless, computer simulations and experiments[15–17] have demonstrated that one of the main effects of the modulational instability is the generation of localized pulses. For example, subpicosecond solitonlike optical pulses have been experimentally generated from a weakly modulated input via an induced modulation instability in single-mode optical fibers.[15] Given this observation, modulational instability recently has been proposed to be a possible mechanism responsible for the energy localization in discrete lattices, and it has been studied in a number of discrete models.[16–23] Although many aspects of MI in discrete systems are the same as those in continuous media, the discreteness can drastically modify the parameter space of modulational instability as deduced from a continuum or even semidiscrete approximation.[19] The advantage of making use of modulational instability to create localized excitations in discrete lattices is that because of the lack of continuous translational symmetry the localized pulse generated by the nonlinear instability can be trapped by discreteness to form strongly localized long-lived excitations.

The analogy between lattice vibrations and spin waves has generated some studies of intrinsic localized spin waves in semiclassical and classical magnetic models.[24–31] The purpose of this paper is to examine the modulational instability of extended nonlinear spin waves in antiferromagnetic chains with easy-axis anisotropy. Previous studies of MI in discrete lattices concerned only *monatomic* lattices with *one* degree of freedom per site. Easy-axis antiferromagnetic chains are equivalent to *diatomic* lattices and have *two* degrees of freedom per site (the length of spin is fixed). In addition, whereas the previously studied Klein-Gordon (KG) lattice and Fermi-Pasta-Ulam lattice have either an on-site anharmonic potential or an intersite anharmonic coupling,[17,19,22] the current model has both nonlinear on-site anisotropy and nonlinear exchange coupling. Here we determine the instability regions by using linear-stability analysis and compare the analytical results with numerical results obtained from molecular-dynamics simulations. We also explore the possibility of generating intrinsic localized spin-wave modes from spatially extended spin waves, and demonstrate that both nonlinearity and discreteness is essential to the creation of long-lived localized excitations.

II. MODULATIONAL INSTABILITY OF NONLINEAR EXTENDED SPIN WAVES

A. Traveling nonlinear extended spin-wave modes

The one-dimensional antiferromagnetic chain of N spins to be investigated is described by the Hamiltonian

$$H = 2J\sum_n \mathbf{S}_n \cdot \mathbf{S}_{n+1} - D\sum_n (S_n^z)^2, \tag{1}$$

where both the exchange constant J and the single-ion anisotropy constant D are positive; hence, the z axis is an easy

axis, and in the ground state adjacent spins point in opposite z directions. Previous studies have demonstrated that intrinsic localized spin-wave modes can exist in the gap below the standard antiferromagnetic resonance frequency.[24,28,30,32]

Each spin moves in the effective magnetic field produced by its two nearest neighbors and the anisotropy field

$$\frac{d\mathbf{S}_n}{dt}=\mathbf{S}_n\times\mathbf{H}_n^{\mathrm{eff}}, \tag{2}$$

where from Eq. (1) the effective magnetic field

$$\mathbf{H}_n^{\mathrm{eff}}=-\nabla_{\mathbf{S}_n}H=-2J(\mathbf{S}_{n-1}+\mathbf{S}_{n+1})+2DS_n^z\mathbf{e}_z.$$

The equations of motion for the circular variable s_n^+, which is defined as $s_n^{\pm}=(S_n^x\pm iS_n^y)/S$ to make use of the axial symmetry of the Hamiltonian, becomes

$$i\,\frac{ds_n^+}{dt}=-2JS[(s_{n-1}^z+s_{n+1}^z)s_n^+-(s_{n-1}^+ +s_{n+1}^+)s_n^z] +2DSs_n^z s_n^+, \tag{3}$$

where S is the magnitude of spin, and the z component of the spins on even sites is chosen to be in the positive z direction. The traveling extended spin-wave mode with wave vector q and frequency ω can be found by substituting into Eq. (3) the following circularly polarized trial solution

$$\begin{aligned} s_{2n}^+(t)&=fe^{i[2nqa-\omega t+\theta_0]},\quad s_{2n}^z=\sqrt{1-f^2}\\ s_{2n+1}^+(t)&=ge^{i[(2n+1)qa-\omega t+\theta_0]},\quad s_{2n+1}^z=-\sqrt{1-g^2}. \end{aligned} \tag{4}$$

Here θ_0 is a constant phase, and both spin deviations f and g are real and nonnegligible. This yields two coupled nonlinear equations

$$\begin{aligned} \Omega f&=2f\sqrt{1-g^2}+(Af+2g\cos qa)\sqrt{1-f^2},\\ \Omega g&=-2g\sqrt{1-f^2}-(Ag+2f\cos qa)\sqrt{1-g^2}, \end{aligned} \tag{5}$$

where the dimensionless frequency $\Omega=\omega/2JS$, and the anisotropy parameter $A=D/J$. Eliminating Ω from Eq. (5) and defining the parameter

$$r=\frac{2}{A+2}, \tag{6}$$

we obtain

$$\frac{g}{f}=-\frac{r\cos qa}{1\pm\sqrt{(1-r^2\cos^2 qa)(1-f^2)}}, \tag{7}$$

where the $\pm$ signs designate two degenerate branches. Owing to the symmetry between the up spins and down spins we can choose the solution with positive sign in the denominator so that $|g/f|<1$ without losing generality. In fact it can be shown that the solution with negative sign in the denominator is equivalent to the one with positive sign after exchanging f and g.

Given the spin-wave amplitude f, the frequency as a function of wave vector can be obtained from Eqs. (5) and (7) as

$$\Omega(q,f)=2\sqrt{1-\alpha^2f^2}+(A-2\alpha\cos qa)\sqrt{1-f^2}, \tag{8}$$

where

$$\alpha=-\frac{g}{f}=\frac{r\cos qa}{1+\sqrt{(1-r^2\cos^2 qa)(1-f^2)}}. \tag{9}$$

Hence the frequency of an extended nonlinear spin wave depends on both its wave vector and its amplitude. In the case of small amplitude $f^2\ll 1$, one finds

$$\Omega(q,f)\approx\Omega_0(q)-\frac{A\Omega_0(q)}{\Omega_0(q)+\Omega_0(\pi/2a)}f^2, \tag{10}$$

where $\Omega_0(q)=\sqrt{(A+2)^2-4\cos^2 qa}$ is the linear spin-wave frequency. Equation (10) indicates that the nonlinear spin-wave frequency decreases quadraticly with increasing amplitude.

B. Modulational instability of extended nonlinear spin waves

To study the modulational stability of the extended nonlinear spin waves, we investigate the time evolution of a perturbed nonlinear spin wave of the form

$$\begin{aligned} s_{2n}^+(t)&=(f+b_{2n}+i\psi_{2n})e^{i[2nqa-\omega t+\theta]},\\ s_{2n+1}^+(t)&=(g+b_{2n+1}+i\psi_{2n+1})e^{i[(2n+1)qa-\omega t+\theta]}, \end{aligned} \tag{11}$$

where f, g, and ω are related by Eqs. (8) and (9), and the perturbations $\{b_n(t)\}$ and $\{\psi_n(t)\}$ are real and are assumed to be small in comparison with the parameters of the carrier wave. Note that in this form we have added the perturbation in a frame rotating with the exact periodic solution. The advantage of the form of Eq. (11) is that it ensures that the resulting linearized equations of the perturbation have constant coefficients instead of time-dependent coefficients as would be obtained in the usual stability analysis of periodic solutions. Since the perturbations $\{b_n(t)\}$ and $\{\psi_n(t)\}$ are arbitrary, so far this does not involve any approximation. Inserting Eq. (11) into Eq. (3) and separating the real and imaginary parts, we obtain, up to the linear terms of $\{b_n(t)\}$ and $\{\psi_n(t)\}$, the four linear equations

$$\frac{1}{2JS}\frac{db_{2n}}{dt}=\{(b_{2n+1}-b_{2n-1})\sin qa+(\psi_{2n+1}+\psi_{2n-1}+2\alpha\psi_{2n})\cos qa\}\sqrt{1-f^2}, \tag{12a}$$

$$\frac{1}{2JS}\frac{db_{2n+1}}{dt}=-\left\{(b_{2n+2}-b_{2n})\sin qa+\left(\psi_{2n+2}+\psi_{2n-1}+\frac{2}{\alpha}\psi_{2n+1}\right)\times\cos qa\right\}\sqrt{1-g^2}, \tag{12b}$$

$$\frac{1}{2JS}\frac{d\psi_{2n}}{dt}=(\psi_{2n+1}-\psi_{2n-1})\sqrt{1-f^2}\,\sin qa + \left\{\frac{gf}{\sqrt{1-g^2}}-\sqrt{1-f^2}\,\cos qa\right\}(b_{2n+1}+b_{2n-1}) - \frac{2\alpha\,\cos qa - Af^2}{\sqrt{1-f^2}}\,b_{2n}, \tag{12c}$$

$$\frac{1}{2JS}\frac{d\psi_{2n+1}}{dt}=-(\psi_{2n+2}-\psi_{2n})\sqrt{1-g^2}\,\sin qa-\left\{\frac{gf}{\sqrt{1-f^2}} - \sqrt{1-g^2}\,\cos qa\right\}(b_{2n+2}+b_{2n}) + \frac{\frac{2}{\alpha}\cos qa - Ag^2}{\sqrt{1-g^2}}\,b_{2n+1}. \tag{12d}$$

To solve the system of coupled linear equations given by Eqs. (12a)–(12d), we expand the perturbation in terms of Fourier components as

$$\begin{pmatrix} b_{2n} \\ \psi_{2n}\end{pmatrix}=\sum_Q \begin{pmatrix} b_0(Q) \\ \psi_0(Q)\end{pmatrix}e^{i2nQa}, \tag{13a}$$

$$\begin{pmatrix} b_{2n+1} \\ \psi_{2n+1}\end{pmatrix}=\sum_Q \begin{pmatrix} b_1(Q) \\ \psi_1(Q)\end{pmatrix}e^{i(2n+1)Qa}. \tag{13b}$$

This decomposition allows us to identify the time evolution of each individual component. Since $\{b_n(t)\}$ and $\{\psi_n(t)\}$ are real,

$$b_i^*(Q)=b_i(-Q),\ \text{ and }\ \psi_i^*(Q)=\psi_i(-Q)\quad (i=0,1). \tag{14}$$

Substituting Eqs. (13a) and (13b) into Eqs. (12a)–(12d) and comparing the coefficients of the same Fourier component, we obtain

$$\frac{d}{dt}\begin{pmatrix} b_0(Q) \\ b_1(Q) \\ \psi_0(Q) \\ \psi_1(Q)\end{pmatrix}=2JS\begin{pmatrix} M_{11} & M_{12} \\ M_{21} & M_{22}\end{pmatrix}\begin{pmatrix} b_0(Q) \\ b_1(Q) \\ \psi_0(Q) \\ \psi_1(Q)\end{pmatrix}, \tag{15}$$

where M_{ij}'s are 2×2 matrices given by

$$M_{11}=\begin{pmatrix} 0 & 2i\sqrt{1-f^2}\,\sin Qa\,\sin qa \\ -2i\sqrt{1-g^2}\,\sin Qa\,\sin qa & 0\end{pmatrix}, \tag{16a}$$

$$M_{11}=M_{22}, \tag{16b}$$

$$M_{12}=\begin{pmatrix} 2\alpha\sqrt{1-f^2}\,\cos qa & 2\sqrt{1-f^2}\,\cos Qa\,\cos qa \\ -2\sqrt{1-g^2}\,\cos Qa\,\cos qa & -\frac{2}{\alpha}\sqrt{1-g^2}\,\cos qa\end{pmatrix}, \tag{16c}$$

$$M_{21}=-M_{12}+\begin{pmatrix} \frac{(A-2\alpha)f^2}{\sqrt{1-f^2}}\cos qa & 2\frac{gf}{\sqrt{1-g^2}}\cos Qa \\ -2\frac{gf}{\sqrt{1-f^2}}\cos Qa & \frac{-(A-2/\alpha)g^2}{\sqrt{1-g^2}}\cos qa\end{pmatrix}. \tag{16d}$$

The general solution of Eq. (15) is a superposition of terms having the time dependence $e^{-i\omega_m t}$ where the ω_m's are the frequencies of the modulation wave relative to the extended nonlinear spin wave and the $-i\omega_m$'s are the eigenvalues of the 4×4 matrix $2JSM$. The stability of the extended nonlinear spin-wave mode is determined by the imaginary part of ω_m. The extended nonlinear spin wave is unstable when the $\mathrm{Im}\{\omega_m\}>0$, otherwise it is stable. Defining the dimensionless frequency $\lambda=\omega_m/2JS$, we can obtain the λ's from

$$\det|\lambda(q,Q)I-iM|=0. \tag{17}$$

Equation (17) determines the condition for the stability of an extended nonlinear spin wave with wave vector q with respect to the modulation with wave vector Q. Since $M_{11}=M_{22}=0$ when $Q=0$, $\lambda(q,0)=0$ is always one of the eigenvalues of matrix M. Note that since the trace of the matrix M is zero regardless of the values of q and Q, the condition for stability is that all eigenvalues of M are imaginary. Otherwise there must be at least one eigenvalue having a positive real part. Furthermore, the symmetric modulation sidebands at $q\pm Q$ have the same growth rate since $\lambda(q,-Q)=-\lambda^*(q,Q)$.

Since there is no simple analytical form for the dispersion relation $\lambda(q,Q)$ for arbitrary q, Eq. (17) has to be solved numerically to determine the domains of instability in the (q,Q) plane. However, two important cases, e.g., the zone center and zone-boundary spin waves, can be solved analyti-

cally. We shall consider these two cases before we consider spin waves with arbitrary wave vectors.

1. The $q=0$ mode

The $q=0$ extended nonlinear spin wave is particularly important in that the existence of the stationary intrinsic localized spin wave gap modes (ILSG's) we previously studied[28] is accompanied by its instability. Hence the condition for instability to occur also tells us when stationary ILSGs can exist. Since $M_{11}=M_{22}=0$ when $q=0$, the case of zone-center spin-wave mode becomes particularly simple. In this case, Eq. (17) becomes

$$\det|\lambda^2(0,Q)I+M_{21}M_{12}|=0, \tag{18}$$

which yields the following dispersion relation for the modulation wave

$$\lambda_{\pm}^2(0,Q)=\left(\alpha C+\frac{B}{\alpha}\right)-4E\ \sin^2\ Qa\pm\left\{\left(\alpha C+\frac{B}{\alpha}\right)^2-4BC\ \sin^2\ Qa\right\}^{1/2}, \tag{19}$$

where

$$B=\frac{2}{\alpha}-(A+2)g^2-2\alpha\sqrt{(1-g^2)(1-f^2)}, \tag{20a}$$

$$C=2\alpha-(A+2)f^2-\frac{2}{\alpha}\sqrt{(1-g^2)(1-f^2)}, \tag{20b}$$

$$E=gf-\sqrt{(1-g^2)(1-f^2)}. \tag{20c}$$

In the case of an isotropic chain ($A=0$), $B=C=0$, and $E=-1$ so that Eq. (19) can be reduced to

$$\lambda_{\pm}^2(Q)=4\sin^2\ Qa. \tag{21}$$

Note that Eq. (21) is merely the linear spin-wave dispersion relation and is positive for any Q. This can be easily understood since the $q=0$ mode in an isotropic chain is simply a rotation of the whole lattice in spin space by an arbitrary amount and any small amplitude perturbation to this state is a superposition of linear spin waves.

In anisotropic antiferromagnetic chains, instability can however occur for the zone-center spin wave. When $A>0$, it is straightforward to show that

$$\alpha C+\frac{B}{\alpha}\geqslant 0, \tag{22a}$$

$$E<0, \tag{22b}$$

$$\left(\alpha C+\frac{B}{\alpha}\right)^2-4BC\ \sin^2\ Qa\geqslant 0. \tag{22c}$$

Hence $\lambda_+^2(0,Q)\geqslant 0$ holds for any Q and this branch is stable. To determine the instability condition we focus on the $\lambda_-(0,Q)$ branch from here on.

It is clear from Eq. (19) that $\lambda_-^2(0,0)=0$ and the instability occurs if and only if $\lambda_-^2(0,Q)$ becomes negative for some nonzero Q. This requires that

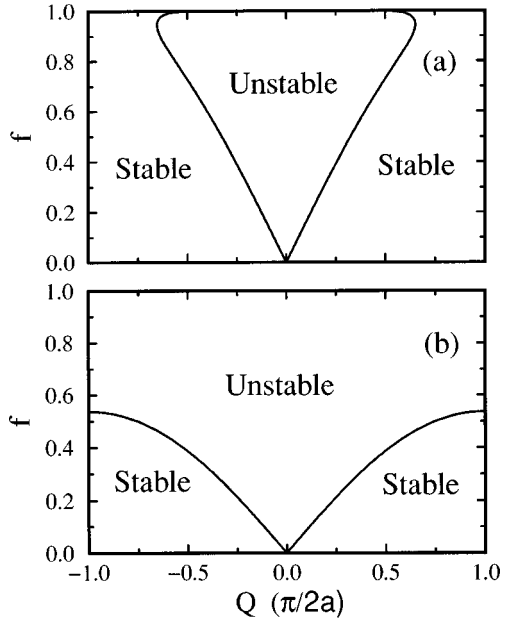

FIG. 1. Regions of modulational instability in the (Q,f) plane for the $q=0$ extended spin wave. (a) The anisotropy parameter $A=1.0$. The large Q region is always stable regardless of the spin-wave amplitude. (b) The anisotropy parameter $A=2.0$. The spin wave with large amplitude becomes unstable to perturbation of any wave vector.

$$\left(\alpha C+\frac{B}{\alpha}\right)-4E\ \sin^2\ Qa<\left\{\left(\alpha C+\frac{B}{\alpha}\right)^2-4BC\ \sin^2\ Qa\right\}^{1/2}. \tag{23}$$

After some algebra the above inequality simplifies to

$$\sin^2\ Qa<\frac{2E(\alpha C+B/\alpha)-BC}{4E^2}. \tag{24}$$

The right-hand side (RHS) of Eq. (24) is always positive for any spin-wave amplitude f, and is proportional to f^2 in the small f limit as shown later. Since in a finite periodic lattice of size N the smallest wave vector is $Q=2\pi/Na$, there exists an amplitude threshold $f_c\sim O(1/N)$ so that only zone center spin waves with amplitude larger than f_c are unstable. However, in a real material $N\sim 10^8$, so the amplitude threshold is negligibly small. The zone-center spin wave is therefore always unstable to long-wavelength modulation, which also means that there is no energy threshold for ILSGs in antiferromagnetic chains since the energy of an unstable nonlinear plane spin wave is proportional to $Nf_c^2\propto 1/N$.[33] One can also show that the RHS of Eq. (24) can become greater than 1 for sufficiently large A and f so that the $q=0$ extended nonlinear spin wave is unstable to any perturbation. When the RHS of Eq. (24) is less than 1 we obtain a critical wave vector given by

$$Q_ca=\arcsin\left[\left(\frac{2E(\alpha C+B/\alpha)-BC}{4E^2}\right)^{1/2}\right]. \tag{25}$$

The extended nonlinear spin-wave mode is unstable to modulation with $|Q|<Q_c$.

As an example the stability region of the $q=0$ extended nonlinear spin wave in the (Q,f) plane is plotted in Fig. 1

for two different anisotropy parameters. In Fig. 1(a) the anisotropy parameter $A=1.0$. The $q=0$ spin wave is stable to modulation waves with large wave vector. When the antiferromagnetic chain becomes more anisotropic with increasing A, the spin wave with large amplitude can become unstable with respect to any modulation wave vector as illustrated in Fig. 1(b) for the case of $A=2.0$.

Equations (19) and (25) hold for arbitrary amplitudes. In the small amplitude limit, they can be simplified to yield more transparent results. Keeping only the lowest terms of f, one can determine from Eq. (25) that

$$Q_c a=\frac{1}{1+\dfrac{\Delta\Omega_0}{2\Omega_0(0)}}\left(\frac{A}{\Delta\Omega_0}\right)^{1/2} f, \tag{26}$$

where $\Delta\Omega_0$ is the bandwidth of the linear spin-wave band, and we have used the approximation $\sin Qa \approx Qa$ for small Qa. The critical wave vector of the modulation wave is therefore linear in the spin-wave amplitude in the small amplitude limit, as can be seen in Fig. 1.

Since the $q=0$ spin wave with a small amplitude is unstable only to long-wavelength ($Qa \sim f$) modulations, Eq. (19) can be simplified in lowest order, i.e., f^4, to yield

$$\lambda_-^2(Q)=-\frac{4(1-r)f^2}{1+\sqrt{1-r^2}}\sin^2 Qa+\frac{r^2}{1-r^2}\sin^4 Qa. \tag{27}$$

The RHS of Eq. (27) is 0 at $Q=0$ and negative for $0<|Q|<Q_c$, hence $\lambda_-(Q)$ is purely imaginary in the small Q region. The maximum growth rate can be found from Eq. (27) to be

$$\mathrm{Im}\{\lambda_-(Q)\}_{\max}=\frac{A}{2}\left(\frac{1}{1+\dfrac{\Delta\Omega_0}{2\Omega_0(0)}}\right)f^2 \tag{28}$$

at the modulation wave vector

$$Q_{\max}=\frac{Q_c}{\sqrt{2}}. \tag{29}$$

The maximum growth rate therefore has a quadratic dependence on the spin-wave amplitude.

2. The zone-boundary mode

Another simple case is the zone-boundary spin wave. At the Brillouin-zone boundary $q=\pi/2a$ and the spin deviation at odd sites $g=0$, hence $\alpha=0$. However the ratio $\cos qa/\alpha$ is well defined, i.e.,

$$\frac{\cos qa}{\alpha}\rightarrow\frac{1+\sqrt{1-f^2}}{r},\quad \text{as } q\rightarrow\frac{\pi}{2a}. \tag{30}$$

Inserting Eq. (30) into Eq. (17), we obtain the following equation for $\lambda(\pi/2a,Q)$:

$$\lambda^4\left(\frac{\pi}{2a},Q\right)+a_2\lambda^2\left(\frac{\pi}{2a},Q\right)+a_0=0, \tag{31}$$

where the coefficients a_0 and a_2 are given by

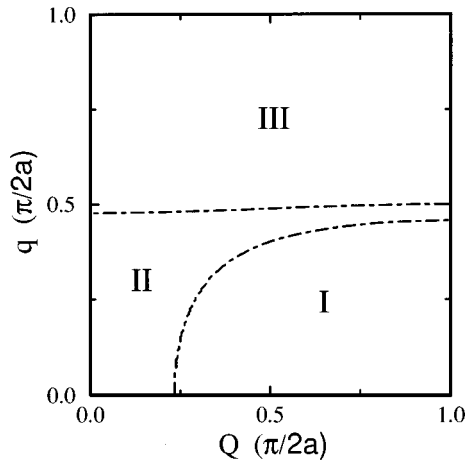

FIG. 2. A typical plot of regions of modulational instability in the (Q,q) plane. Regions I and III are stable regions, and region II is unstable. Spin waves with a wave vector larger than $\pi/4a$ are stable to a perturbation of any wave vector.

$$a_0=16(1-f^2)\sin^4 Qa+\frac{8A}{r}f^2(1+\sqrt{1-f^2})\sin^2 Qa, \tag{32a}$$

$$a_2=-\frac{4}{r^2}(1+\sqrt{1-f^2})^2+8\sqrt{1-f^2}\sin^2 Qa. \tag{32b}$$

Therefore the dispersion relation of perturbation waves $\lambda(\pi/2a,Q)$ can be presented as

$$\lambda_\pm^2\left(\frac{\pi}{2a},Q\right)=\frac{-a_2\pm\sqrt{a_2^2-4a_0}}{2}. \tag{33}$$

Since $a_2<0$ and $a_0\geq 0$, the condition for stability becomes $a_2^2-4a_0\geq 0$, which leads to

$$\frac{(1+\sqrt{1-f^2})^3}{r^4}-\left[\frac{4}{r^2}(1+\sqrt{1-f^2})-\frac{4}{r}f^2\right]\sin^2 Qa\geq 0. \tag{34}$$

It can be readily shown that the inequality given by Eq. (34) holds for any Q and f since $\sin^2 Qa\leq 1$. Hence the extended nonlinear spin waves at the Brillouin-zone boundary are stable to perturbations by any wave vector.

3. Instability region of spin waves with arbitrary q

For nonlinear spin waves of arbitrary wave vector q the dispersion relation $\lambda(q,Q)$ has to be obtained by numerically solving Eq. (17). Figure 2 shows a typical plot of the regions of modulational instability in the (Q,q) plane that is determined by $\mathrm{Im}\{\lambda(q,Q)\}$ for an anisotropic antiferromagnetic chain. The dot-dashed lines separate the regions of stability (I and III) and region of instability (II). In regions I and III $\mathrm{Im}\{\lambda(q,Q)\}\leq 0$ for any of the four $\lambda(q,Q)$'s corresponding to the same pair of (q,Q), while in region II at least one of the four $\lambda(q,Q)$'s has a positive imaginary part. For a given spin-wave amplitude f, the area of the instability region grows increasing anisotropy parameter A. The lower boundary moves towards the direction of large Q, while the upper boundary approaches $q=\pi/4a$. However, spin waves with $q>\pi/4a$ are stable against any perturbation indepen-

dent of the values of Q and f. On the other hand, as the chain becomes more and more isotropic with A approaching zero, the area of the instability region shrinks until it disappears for the isotropic chain.

A number of studies of various lattice dynamical models have shown that the existence of intrinsic localized modes is always accompanied by the instability of corresponding extended nonlinear waves.[18–20,23] Previous study has shown that the intrinsic localized spin waves (ILSMs) can occur only in the gap below the standard antiferromagnetic resonance frequency at $q=0$ while no ILSM exists at the Brillouin-zone boundary.[28] This is in agreement with Fig. 2 where only extended spin waves with small q are unstable to a long-wavelength modulation while the zone-boundary spin waves are stable to the modulation of any wavelength.

III. COMPARISON BETWEEN NUMERICAL SIMULATIONS AND ANALYTICAL RESULTS

According to the above analytical results based on linear-stability analysis, in an easy-axis antiferromagnetic chain the stability of an extended nonlinear spin wave with wave vector q modulated by a small-amplitude wave of wave vector Q is determined by the dispersion relation $\lambda(q,Q)$ that can be obtained from Eq. (17). Linear stability analysis can determine the instability domain in parameter space and predict quantitatively how the amplitude of a modulation sideband evolves at the onset of the instability; however, such analysis is based on the linearization around the unperturbed carrier wave, which is valid only when the amplitude of perturbation is small in comparison with that the carrier wave. Clearly, the linear approximation must fail at large time scales as the amplitude of unstable sideband grows exponentially. Furthermore, the linear-stability analysis neglects additional combination waves generated through wave-mixing processes which, albeit small at the initial stage, can become significant at large time scales if its wave vector falls in an instability domain. Linear-stability analysis therefore cannot tell us the long-time evolution of a modulated extended nonlinear spin wave. In order to check the validity of our analytical analysis and to investigate the long-time evolution of modulated nonlinear spin waves, we have carried out molecular dynamics simulations for easy-axis chains with various anisotropy parameters.

In our numerical simulations the initial conditions are coherently modulated extended nonlinear spin waves of the form

$$s_{2n}^{+}(0)=\left\{f+\frac{\beta}{2}\left[b_0(Q)e^{i2nQa}+\text{c.c.}+i(\psi_0(Q)e^{i2nQa}+\text{c.c.})\right]\right\}e^{i2nqa},$$
$$s_{2n+1}^{+}(0)=\left\{g+\frac{\beta}{2}\left[b_1(Q)e^{i(2n+1)Qa}+\text{c.c.}+i(\psi_1(Q)e^{i(2n+1)Qa}+\text{c.c.})\right]\right\}e^{i(2n+1)qa}, \tag{35}$$

where c.c. denotes the complex conjugate, $(b_0(Q),\ b_1(Q),\ \psi_0(Q),\ \psi_1(Q))$ is a normalized eigenvector of the M matrix, and β is a small parameter measuring the relative strength of the modulation wave to the carrier wave, typically at the order of 0.01. The amplitudes f and g are related by Eq. (7). Since $|b+i\psi|^2\neq|b^*+i\psi^*|^2$, the two satellites at $q\pm Q$ have different strengths except when $q=0$. Given $s_n^+(0)$, the z components of spins can be obtained from

$$s_n^z(0)=(-1)^n\sqrt{1-|s_n^+(0)|^2}. \tag{36}$$

Once an initial condition is given the time evolution of a modulated spin wave can be investigated by means of molecular-dynamics (MD) simulations. In order to monitor the time evolution of individual Fourier components, we define the complete spatial Fourier transform of spin deviations

$$m(p,t)=\sum_{n=0}^{N-1}s_n^+(t)e^{-in(2p\pi/N)},\quad\left(-\frac{N}{4}<p\leq\frac{N}{4}\right). \tag{37}$$

The growth rate of each individual Fourier component can be obtained by the least square fitting of $|m(p,t)|^2$ over the first few periods during which time it is expected to grow at the rate of 2 Im$\{\lambda(q,Q)\}$.

As a specific example, we first consider a chain of 128 spins with periodic boundary conditions. The anisotropy parameter is taken to be $A=1.0$, and the spin-wave amplitude $f=0.2$. Figure 3 shows the long-time evolution of the carrier wave with wave vector $q=15\pi/64a$ modulated by small amplitude waves with wave vectors $Q=\pm17\pi/64a$ that falls in the unstable region. The exponential growth of $q\pm Q$ satellite sidebands at the initial stage of instability is obvious as can be seen in the log-linear plot of Fig. 3(a). Figure 3(b) shows the time evolution of the complete Fourier spectrum where additional combination waves generated from wave-mixing processes can be seen after about $300T_{\text{AFMR}}$ as the instability further develops.

Plotted in Fig. 4 are the growth rates as a function of the modulation wave vector for the running carrier waves with various wave vectors. The solid curves represent analytical results obtained by diagonalizing the matrix M while the filled circles are MD simulation results. The excellent agreement between them demonstrates that the linear-stability analysis does give a quantitatively correct description of the onset of instability. An interesting feature can be seen in Fig. 4. While the carrier waves with small q are unstable to long-wavelength modulation (small Q), a carrier wave of large q $(q=15\pi/64a)$ is stable to long-wavelength modulations but unstable to some short-wavelength modulations (large Q). This is in contrast to what was reported in Ref. 19 for a monatomic Klein-Gordon chain that is also subject to an on-site anharmonic substrate potential. In the Klein-Gordon

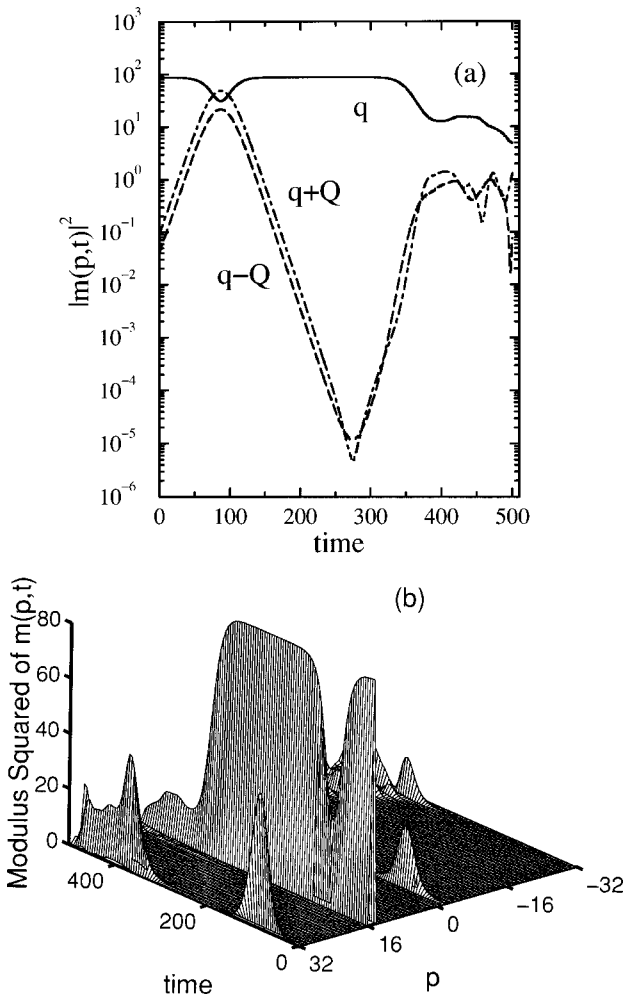

FIG. 3. Time evolution of the carrier wave with $q=15\pi/64a$ and $f=0.2$ modulated by a small amplitude wave with $Q=17\pi/64a$. The anisotropy parameter is $A=1.0$, and time is measured in units of T_{AFMR}, the period of the $q=0$ linear spin wave. (a) Time evolution of the main Fourier components at q (solid curve), $q+Q$ (dot-dashed curve) and $q-Q$ (long-dashed curve). (b) Time evolution of the complete Fourier spectrum. After a sufficiently long time, combination modes appear.

chains the small Q region is always the unstable region as long as an instability does occur for the corresponding carrier wave.

The prediction of stability from linear analysis does not necessarily rule out the occurrence of instability in the long-time evolution because of the combination waves neglected there. To illustrate this point, the long-time evolution of a perturbed carrier wave with wave vector $q=15\pi/64a$ is plotted in Fig. 5. In this case the modulation wave vectors $Q=\pm\pi/8a$ lie in the stable region as shown in Fig. 4(a). The Fourier component corresponding to the carrier wave remains the same for a period of approximately $180T_{\mathrm{AFMR}}$ before the instability occurs. From the time evolution of the spatial Fourier components at wave vectors q, $q\pm Q$, and $q\pm 2Q$ plotted in Fig. 5(a), it can be seen that the $q\pm Q$ components do not grow until after $t=180T_{\mathrm{AFMR}}$, just as predicted in the linear-stability analysis, but the $q\pm 2Q$ components which are neglected in the linear-stability analysis grow to significant magnitudes after $180T_{\mathrm{AFMR}}$. Consequently, the carrier wave becomes unstable and generates even more combination modes.

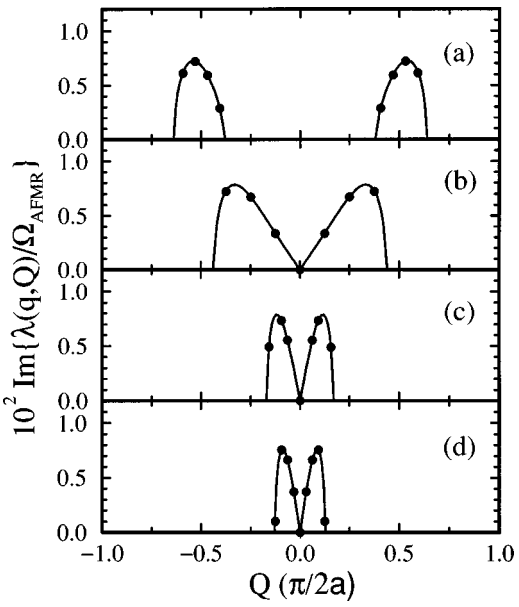

FIG. 4. Growth rate of modulational waves as a function of modulation wave vector for carrier waves with various wave vectors. The parameters are $A=1.0$ and $f=0.2$. Ω_{AFMR} is the standard antiferromagnetic resonance frequency. The wave vectors of carrier waves are: (a) $15\pi/64a$, (b) $7\pi/32a$, (c) $\pi/8a$, and (d) 0. The solid curves are analytical results while the filled circles are MD simulation results.

This simulation demonstrates that the combination modes at $q\pm 2Q, q\pm 3Q$ generated by the nonlinearity, though their magnitudes are smaller than that of the $q\pm Q$ by at least a factor β at $t=0$, may fall in the instability region and play an important role at sufficiently large time scales. Hence the condition for stability for large time scales is that not only the main satellite modulation but also all combination modes must not lie in the regions of instability. Note that unlike in other models such as the Klein-Gordon lattice and Fermi-Pasta-Ulam lattice, the nonlinearity in the uniaxial easy-axis antiferromagnetic chains does not generate combination waves at $\pm 2q, \pm 3q, \ldots$, etc. With the Brillouin-zone folding back taken into account, the stability condition is given by

$$\mathrm{mod}\left(q\pm nQ, \frac{\pi}{a}\right) \notin \textit{unstable regions}, \quad n=1,2,\ldots . \tag{38}$$

According to Fig. 2, this condition is quite restrictive and it appears that only carrier waves with wave vector $q>\pi/4a$ are stable on large time scales.

As the anisotropy parameter increases the antiferromagnetic chain appears more discrete and according to the analytical results the area of the instability region in the (Q,q) plane also grows so that the upper boundary of the instability region in Fig. 2 approaches $q=\pi/4a$. As an example we investigate a chain with a larger anisotropy parameter. As in the first example the chain contains 128 spins with periodic boundary conditions but the anisotropy parameter is taken to be $A=2.0$. The amplitudes of the extended nonlinear carrier waves are still $f=0.2$. The growth rates of the amplitude of

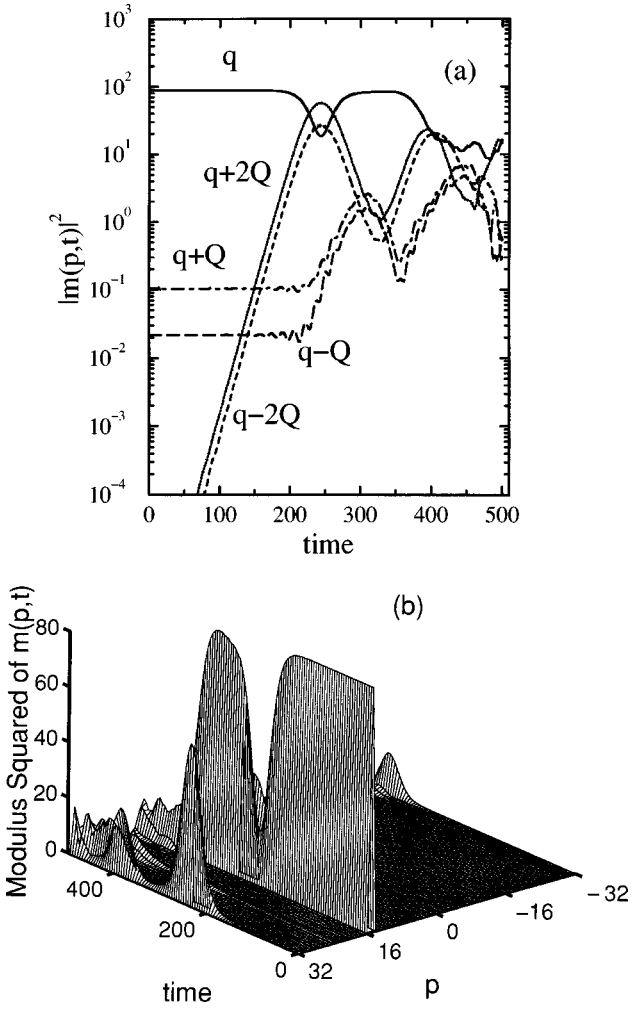

FIG. 5. Instability induced by combination modes. The wave vector and amplitude of the carrier wave are $q=15\pi/64a$ and $f=0.2$, respectively. The modulation wave vector $Q=\pi/8a$ lies in the stable region, as can be seen in Fig. 3(a). Time is measured in units of T_{AFMR}. (a) Time evolution of the Fourier components at q (solid curve), $q+Q$ (dot-dashed curve), $q-Q$ (long-dashed curve), $q+2Q$ (doted curve) and $q-2Q$ (short-dashed curve). (b) Time evolution of the complete Fourier spectrum.

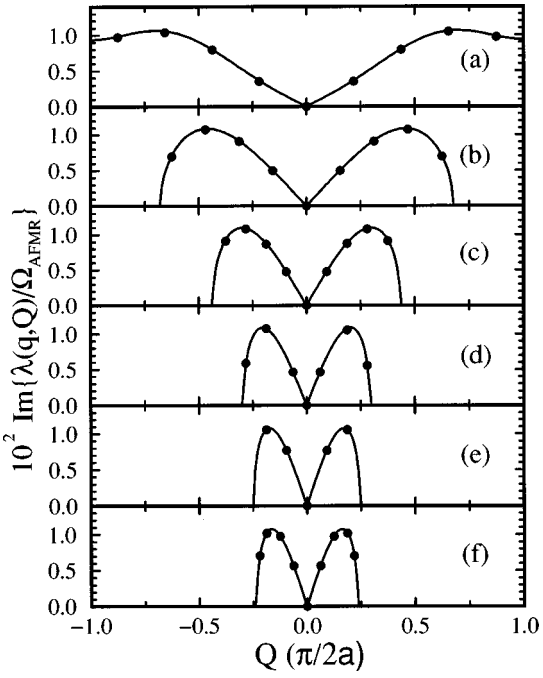

FIG. 6. Growth rate of modulational waves as a function of the modulation wave vector in an antiferromagnetic chain with large anisotropy. The parameters are $A=2.0$ and $f=0.2$, and Ω_{AFMR} is the standard antiferromagnetic resonance frequency. Solid curves are analytical results while filled circles are MD simulation results. The wave vector of carrier waves are: (a) $15\pi/64a$, (b) $7\pi/32$, (c) $3\pi/16$, (d) $\pi/8$, (e) $\pi/16$, and (f) 0. Note that the carrier wave with $q=15\pi/64a$ is unstable to perturbation of any wave vector.

modulation waves for carrier waves with a wide range of wave vectors are plotted in Fig. 6. The MD simulation results (filled circles) are in excellent agreement with the analytical results. The instability region steadily grows with increasing carrier wave wave vector, and the carrier wave with $q=15\pi/64a$ is unstable to modulation by any wave vector. However, if the carrier wave wave vector increases beyond $q=\pi/4a$, it becomes stable to modulation by any wave vector.

IV. CREATION OF INTRINSIC LOCALIZED SPIN-WAVE MODES

A. Lossless system

In the previous sections numerical simulations have demonstrated that the energy initially concentrated in one unstable mode will finally flow to all available modes in Fourier space, e.g., the energy is delocalized in Fourier space. Since a delocalized state in Fourier space can be either a localized state or a delocalized state in the corresponding real space, depending on the relative phases between Fourier components, the time evolution in Fourier space alone does not tell us the complete process of energy redistribution. It is generally believed that the system will finally reach equipartition of energy in a sufficiently long time since entropy should grow during the system's time evolution. In other words the system should approach a state where the energy is evenly distributed not only among modes in Fourier space but also on lattice sites in real space. However, this does not exclude the possibility of energy localization at intermediate stages. Indeed, one of the main effects of modulational instability is the creation of localized excitations from spatially extended excitations.[15] This modulational-instability-induced energy localization has been proposed to be the mechanism responsible for the formation of intrinsic localization.[15,17,19,20,34] For instance, it has been demonstrated in computer simulations that modulational instability can be used to generate intrinsic localized vibrational modes via an optimal control scheme.[34]

Here we investigate how the energy initially concentrated in one mode is redistributed in an antiferromagnetic chain. The time evolution of a zone-center mode perturbed by random noise in both Fourier space and real space is plotted in Fig. 7. The chain consists of 128 spins with anisotropy parameter $A=2.0$. The amplitude of the zone-center spin wave is $f=0.2$, and the amplitude of noise perturbation is small compared to that of the carrier wave, i.e., $|\delta s_n^+(0)/s_n^+(0)|<0.01$. In Fig. 7(a) the time evolution of the complete Fourier spectrum shows that the $q=0$ mode remains stable for a

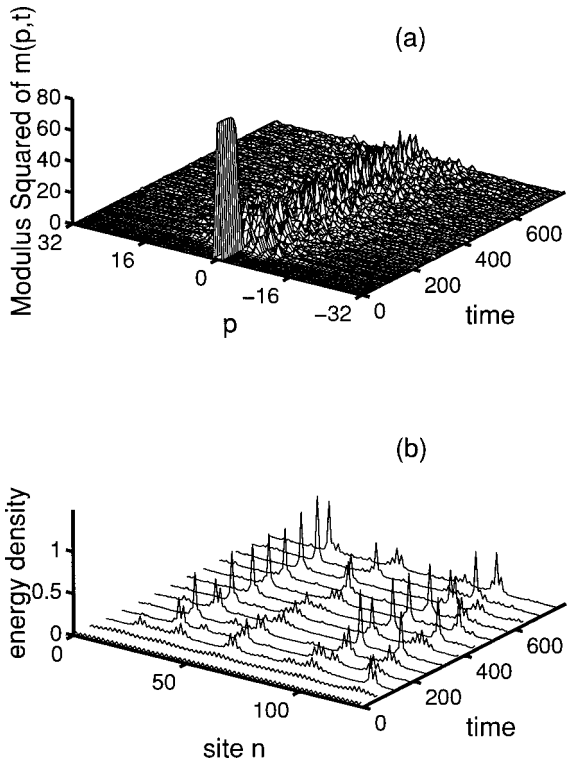

FIG. 7. Creation of intrinsic localized spin-wave excitations from extended nonlinear spin waves via modulational instability. The anisotropy parameter is $A=2.0$. Initially the $q=0$ extended spin wave with amplitude $f=0.2$ is perturbed by random noise. Time is measured in units of T_{AFMR}, and energy is measured from ground state in units of $2JS$. (a) Time evolution of the perturbed spin wave in Fourier space. (b) Time evolution of the energy density distribution in real space.

short period of time (about $80T_{\mathrm{AFMR}}$) then quickly decays into other Fourier components, i.e., the energy is delocalized in Fourier space. In Fig. 7(b), the time evolution of the energy density distribution defined as

$$e(n,t)=J\mathbf{S}_n\cdot(\mathbf{S}_{n-1}+\mathbf{S}_{n+1})-D(S_n^z)^2 \tag{39}$$

in real space shows a different picture. The initial uniformly distributed energy becomes localized as the instability develops. A number of localized excitations are created and appear to be trapped by the discreteness of the lattice. These localized excitations appear to last for a time scale sufficiently long for experimental purpose, as demonstrated in this numerical simulation.

From the above numerical simulation it appears possible to create strongly localized long-lived excitations by driving the antiferromagnetic chain into a nonlinear regime[17] using optimal control schemes with powerful laser pulses, such as the one reported in Ref. 34. However, our numerical experiments with different anisotropy parameters and carrier wave amplitudes demonstrate that although localized excitations can be created in this way their lifetimes depend strongly on the anisotropy parameter of the lattice and the amplitude of the initial carrier wave. Since the anisotropy here is on-site, it is not only a measure of the anharmonicity but also an effective measure of the discreteness of the lattice. As the anisotropy parameter A or the carrier wave amplitude decreases, i.e., the lattice is less discrete and less anharmonic, and the lifetime of localized excitations decreases. To obtain a more quantitative characterization, we define the energy-energy correlation function as[17,35]

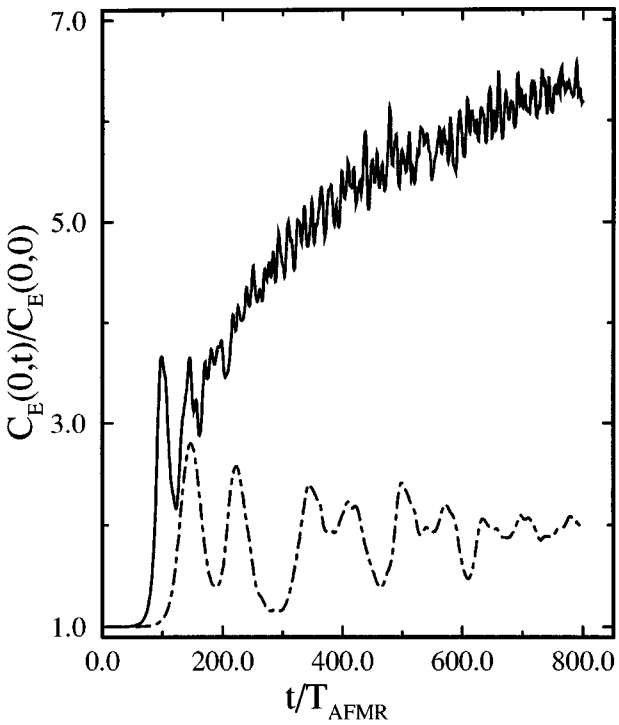

FIG. 8. The height of the center spike of the energy-energy correlation function as a function of time. Initially the $q=0$ extended spin wave with amplitude $f=0.2$ is perturbed by random noise. Solid curve: $A=2.0$. Dot-dashed curve: $A=1.0$. Each curve is averaged over 20 initial conditions.

$$C_E(n,t)=N\left\langle \frac{\sum_m e(m,t)e(m+n,t)}{\left[\sum_m e(m,t)\right]^2}\right\rangle , \tag{40}$$

where $\langle\cdots\rangle$ indicates the average over initial conditions. For a uniform energy distribution, such as our initial conditions, $C_E(n)$ is just a uniform background, while when localized excitations appear $C_E(n)$ should consist of a central spike. Since the total energy is a conserved quantity, the degree of localization can be measured by the height (or the width) of the central spike.

To illustrate the effect of the anisotropy parameter on the energy localization process of randomly perturbed nonlinear plane spin waves, the height of the central spike of the energy-energy correlation function as a function of time is plotted in Fig. 8 for two antiferromagnetic chains with anisotropy parameters $A=1.0$ and 2.0, respectively. In both cases, the carrier waves have the same amplitude and wave vector, i.e., $q=0$ and $f=0.2$, and each curve is averaged over 20 initial conditions. Note that the solid curve ($A=2.0$) is qualitatively different from the dot-dashed curve ($A=1.0$). In the case of the larger anisotropy parameter, the height of the central spike in the energy-energy correlation function increases with time during the simulation period, which indicates that localized excitations are generated and

grow with time. Although localized excitations are also generated in the lattice with a smaller anisotropy parameter, they are short lived and the energy appears to be exchanged back and forth between localized excitations and extended spin waves. This demonstrates that the discreteness *and* strong anharmonicity seem to be essential for the creation of long-lived localized excitations.

Ignoring the difference between the three-dimensional (3D) and 1D lattices examples of the modulational instability effect described above may be displayed by well-known uniaxial systems.[36] Because of its relatively weak anisotropy field, MnF_2 should generate localized excitations only on a short-time scale. On the other hand, FeF_2, with the much larger anisotropy value, would be expected to produce localization on a much longer time scale. Even though we have not treated easy plane antiferromagnets here, a general statement can be made about their expected instabilities. Systems such as MnO and NiO should not show this long-lived localized behavior because of the underlying weak localization associated with the production of nonlinear resonant modes.[29]

B. System with dissipation

So far we have investigated the modulational instability of nonlinear spin waves and the creation of ILSMs in lossless easy-axis antiferromagnetic chains. In this section we shall discuss the influence of weak dissipation.

In a dissipative chain, the equations of motion represented by Eq. (2) become

$$\frac{d\mathbf{S}_n}{dt}=\mathbf{S}_n\times\mathbf{H}_n^{\mathrm{eff}}-\varepsilon\mathbf{S}_n\times(\mathbf{S}_n\times\mathbf{H}_n^{\mathrm{eff}}), \tag{41}$$

where the second term is the Landau-Gilbert damping[36] that preserves the spin length, and ϵ is a small parameter measuring the damping strength. The dissipation in magnetic materials is usually weak, for instance, $\Gamma/\omega\sim10^{-5}$ in bulk MnF_2 (Ref. 37) and FeF_2 (Ref. 38) and $\sim10^{-4}$ in ferromagnetic yttrium-iron-garnet films.[39] For the case of weak dissipation the amplitude decay rate Γ of plane spin waves is from Eq. (41)

$$\Gamma(q)=2JS^2(A+2)\varepsilon+O(\varepsilon f^2). \tag{42}$$

The dissipation imposed amplitude threshold f_{th} follows from the condition that the maximum MI growth rate be greater than the damping rate. From Eqs. (28) and (42), one obtains

$$f_{\mathrm{th}}^2=\frac{2(A+2)S}{A}\left(1+\frac{\Delta\Omega_0}{2\Omega_0(0)}\right)\varepsilon. \tag{43}$$

It should however be pointed out that Eq. (43) does not guarantee the formation of ILSMs from the MI. The formation of ILSMs is a dynamical process in which the competing effects of nonlinearity and dispersion reach a delicate balance. The characteristic time scale of this nonlinear process can be obtained from the nonlinear frequency shift given in Eq. (10), that is,

$$T_{\mathrm{NL}}=\frac{2\pi}{|\Delta\omega|}=\frac{\Omega_0(q)+\Omega_0(\pi/2a)}{Af^2}\,T_{\mathrm{AFMR}}. \tag{44}$$

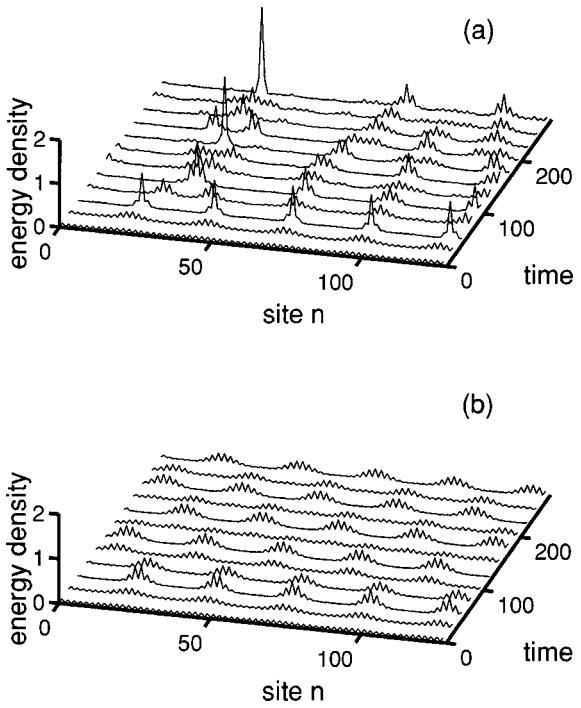

FIG. 9. The influence of weak dissipation on ILSMs' formation from modulational instability for two different damping factors. The energy density is multiplied by $e^{2\Gamma t}$ for ease in viewing. Initially the $q=0$ extended spin wave with amplitude $f=0.2$ is perturbed in a lattice with $A=2.0$. (a) $\Gamma/\omega_0(0)=10^{-4}$. (b) $\Gamma/\omega_0(0)=10^{-3}$.

With the parameters $A=2.0$ and $f=0.2$ used in our numerical simulations, one finds $T_{\mathrm{NL}}\approx93T_{\mathrm{AFMR}}$. ILSMs can be created from the MI only when effects of nonlinearity and dispersion are much stronger than the dissipation effect,[40] the condition is that

$$\Gamma(q)T_{\mathrm{NL}}\ll1. \tag{45}$$

To illustrate the influence of weak dissipation on the formation of ILSMs, MD simulations with the perturbed $q=0$ extended spin wave with amplitude $f=0.2$ as initial condition were carried out and the time evolution of the energy distribution were obtained for two different dissipation values. The energy density multiplied by $e^{2\Gamma t}$, for ease in viewing, is plotted in Fig. 9(a) for $\Gamma/\omega_0(0)=10^{-4}$ and Fig. 9(b) for $\Gamma/\omega_0(0)=10^{-3}$. Interesting differences can be found between the two cases. The ILSMs in the weaker dissipation case are much more localized and appear to be pinned but less strongly than the case for no dissipation previously shown in Fig. 7(b). On the other hand, the ILSMs in the stronger dissipation case [Fig. 9(b)] are more delocalized and hence more mobile. This difference results from the competition between the MI-induced energy localization and the dissipation effect. In the weaker dissipation case ($\Gamma T_{\mathrm{NL}}\approx0.058$) the MI process can take place before dissipation becomes significant, while in the stronger dissipation case ($\Gamma T_{\mathrm{NL}}\approx0.58$) the dissipation effect prevents energy from strongly localized by decreasing the amplitude and hence reducing the strength of the nonlinearity.

V. CONCLUSIONS

We have investigated the modulational instability of extended nonlinear spin waves in antiferromagnetic chains with on-site easy-axis anisotropy. The model is equivalent to a ''diatomic'' lattice with two degrees of freedom per site and involves both on-site and intersite nonlinearity. The instability domain in parameter space is determined from linear-stability analysis. Although nonlinear plane spin waves with short wavelengths ($q>\pi/4a$) are stable to any noise perturbation, spin waves with long wavelengths ($q<\pi/4a$) can be unstable to modulation by certain wave vectors and the instability domain in (q,Q) plane grows with increasing the anisotropy parameter or the spin-wave amplitude. In contrast to the monatomic KG chain[19] where plane waves with wave vectors in the lower half of Brillouin zone are always unstable to long-wavelength perturbations, in easy-axis antiferromagnetic chains spin waves with wave vectors close to the zone center (but $q<\pi/4a$) are stable to both long-wavelength and short-wavelength perturbations but unstable to perturbations of moderate wavelengths. The amplitude threshold for the instability of long-wavelength spin waves is inversely proportional to the lattice size, and therefore tends to zero in real materials. The analytic results are compared to numerical simulations and good agreement is obtained. Since the long-time evolution of nonlinear spin waves are analytically untractable, numerical simulations are employed. It reveals that combination waves generated via wave-mixing processes can have significant effect on the spin-wave stability at large time scale. One of the main effects of the modulational instability is the creation of localized pulses and hence it provides a possible mechanism for the generation of intrinsic localized spin waves. Weak dissipation produces two interesting features absent in lossless lattices: it imposes a finite amplitude threshold even for infinite chains and the ILSMs become mobile during formation because of the reduced strength of the nonlinearity. Our numerical experiments demonstrate that the combination of discreetness and a strong nonlinearity is essential for the creation of long-lived ILSMs.

ACKNOWLEDGMENTS

Discussions with S. A. Kiselev are appreciated. This work was supported in part by NSF-DMR-9631298, ARO-DAAH04-96-1-0029, and the MRL central facilities. Some of this research was conducted using the resources of the Cornell Theory Center, which receives major funding from the National Science Foundation and New York State.

[1] A. S. Dolgov, Fiz. Tverd. Tela **28**, 1641 (1986) [Sov. Phys. Solid State **28**, 907 (1986)].
[2] A. J. Sievers and S. Takeno, Phys. Rev. Lett. **61**, 970 (1988).
[3] V. M. Burlakov, S. A. Kiselev, and V. N. Pyrkov, Phys. Rev. B **42**, 4921 (1990).
[4] J. B. Page, Phys. Rev. B **41**, 7835 (1990).
[5] A. J. Sievers and J. B. Page, in *Dynamical Properties of Solids*, edited by G. K. Horton and A. A. Maradudin (North-Holland, Amsterdam, 1994), Vol. 7, p. 137.
[6] S. Aubry, Physica D **103**, 201 (1997).
[7] S. Flach and C. R. Willis, Phys. Rep. (to be published).
[8] R. S. MacKay and S. Aubry, Nonlinearity **7**, 1623 (1994).
[9] S. Aubry and G. Abramovici, Physica D **43**, 199 (1990).
[10] S. Aubry, Physica D **71**, 196 (1994).
[11] T. B. Benjamin and J. E. Feir, J. Fluid Mech. **27**, 417 (1967).
[12] T. Taniuti and H. Washimi, Phys. Rev. Lett. **21**, 209 (1968).
[13] A. Hasegawa, *Optical Solitons in Fibers* (Springer, New York, 1989).
[14] P. Marquie, J. M. Bilbault, and M. Remoissenet, Phys. Rev. E **49**, 828 (1994).
[15] K. Tai, A. Tomita, J. L. Jewell, and A. Hasegawa, Appl. Phys. Lett. **49**, 236 (1986).
[16] J. M. Bilbault and P. Marquie, Phys. Rev. E **53**, 5403 (1996).
[17] I. Daumont, T. Dauxois, and M. Peyrard, Nonlinearity **10**, 617 (1997).
[18] V. M. Burlakov and S. A. Kiselev, Zh. Eksp. Teor. Fiz. **99**, 1526 (1991) [Sov. Phys. JETP **72**, 854 (1991)].
[19] Y. S. Kivshar and M. Peyrard, Phys. Rev. A **46**, 3198 (1992).
[20] Y. S. Kivshar, Phys. Rev. E **48**, 4132 (1993).
[21] Y. S. Kivshar and M. Salerno, Phys. Rev. E **49**, 3543 (1994).
[22] V. M. Burlakov, S. A. Darmanyan, and V. N. Pyrkov, Phys. Rev. B **54**, 3257 (1996).
[23] K. W. Sandusky and J. B. Page, Phys. Rev. B **50**, 866 (1994).
[24] S. Takeno and K. Kawasaki, Phys. Rev. B **45**, R5083 (1992).
[25] S. Takeno and K. Kawasaki, J. Phys. Soc. Jpn. **63**, 1928 (1994).
[26] R. F. Wallis, D. L. Mills, and A. D. Boardman, Phys. Rev. B **52**, R3828 (1995).
[27] S. Rakhmanova and D. L. Mills, Phys. Rev. B **54**, 9225 (1996).
[28] R. Lai, S. A. Kiselev, and A. J. Sievers, Phys. Rev. B **54**, R12 665 (1996).
[29] R. Lai and A. J. Sievers, Phys. Rev. B **55**, R11 937 (1997).
[30] J. Ohishi, M. Kubota, K. Kawasaki, and S. Takeno, Phys. Rev. B **55**, 8812 (1997).
[31] R. Lai, S. A. Kiselev, and A. J. Sievers, Phys. Rev. B **56**, 5345 (1997).
[32] R. Lai and A. J. Sievers, J. Appl. Phys. **81**, 3972 (1997).
[33] S. Flach, K. Kladko, and R. S. MacKay, Phys. Rev. Lett. **78**, 1207 (1997).
[34] T. Rossler and J. B. Page, Phys. Rev. Lett. **78**, 1287 (1997).
[35] D. W. Brown, L. J. Bernstein, and K. Lindenberg, Phys. Rev. E **54**, 3352 (1996).
[36] A. H. Morrish, *The Physical Principles of Magnetism* (Wiley, New York, 1965), p. 623.
[37] J. P. Kotthaus and V. Jaccarino, Phys. Rev. Lett. **28**, 1649 (1972).
[38] R. W. Sanders, R. M. Belanger, M. Motokawa, V. Jaccarino, and S. M. Rezende, Phys. Rev. B **23**, 1190 (1980).
[39] A. N. Slavin, Phys. Rev. Lett. **77**, 4644 (1996).
[40] A. N. Slavin, B. A. Kalinikos, and N. G. Kovshikov, in *Nonlinear Phenomena and Chaos in Magnetic Materials*, edited by P. E. Wigen (World Scientific, Singapore, 1994).